

# **Thermophoretically driven capillary transport of nanofluid in a microchannel with particle deposition**

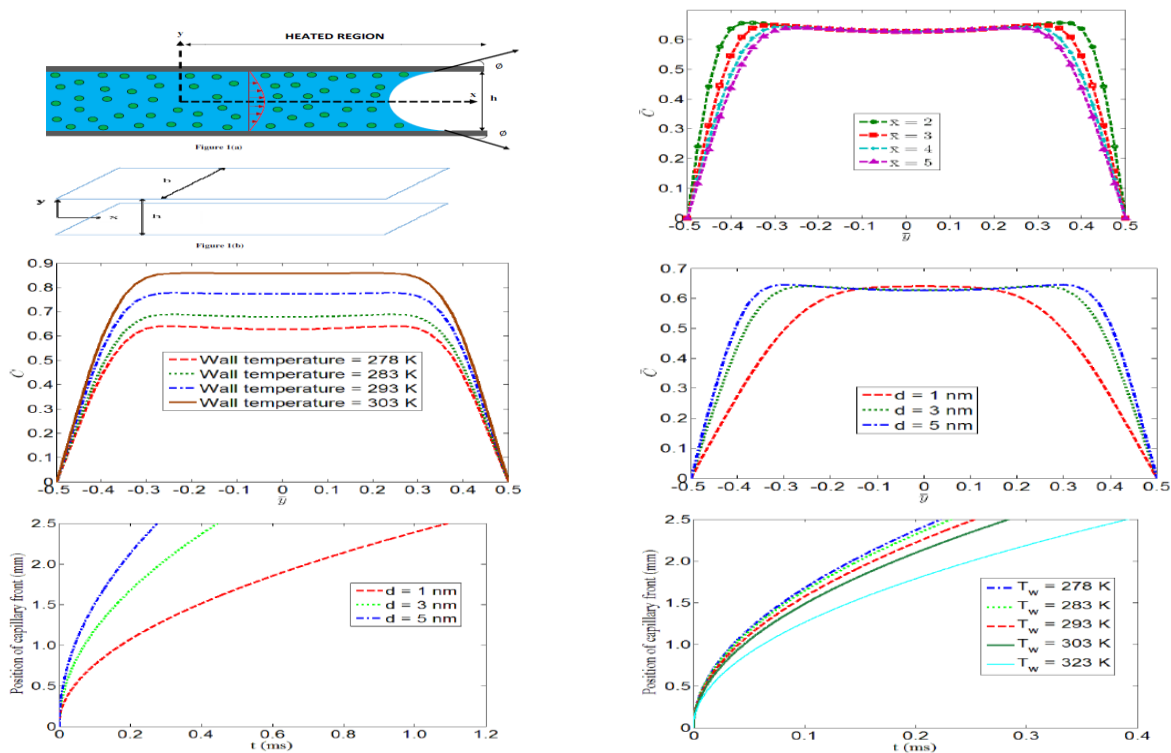
Soumya Bandyopadhyay and Suman Chakraborty

*Department of Mechanical Engineering, Indian Institute of Technology Kharagpur, West Bengal, India – 721302*

## **HIGHLIGHTS**

- Influence of thermal gradient and particle size on thermophoretically driven capillary transport of nanofluid is investigated.
- Thermal gradient increases nanoparticle deposition, reducing the particle bearing efficacy of a nanofluid.
- With increase in particle size, there is a transition from diffusion-dominated particle deposition to thermophoretically dominated deposition, for a given temperature field.
- Both thermal gradient and particle size enhance rate of capillary transport.
- Optimum flow rates for a given nanofluid can be achieved by appropriately adjusting thermal gradients, rendering energy efficient engineering systems.

# GRAPHICAL ABSTRACT



# ABSTRACT

We investigate the interplay of thermophoretic force and interfacial tension on the capillary filling dynamics of a Newtonian nanofluid in a microchannel. In our model, we also consider an intricate thermofluidic coupling by taking the temperature dependence of viscosity aptly into account. This, in turn, determines the evolution of the viscous resistive force as the capillary front progresses, and presents an involved inter-connection between the driving thermophoretic force and the viscous resistive force. The two distinct regimes of particle transport in fluid medium, delineated by particle size, are expounded to peruse the impact of imposed thermal gradients and particle size on particle retaining propensity of the nanofluid. Additionally, we witness significant reduction in particle bearing proclivity of the nanofluid with enhancement in thermal gradient. The results demonstrate the efficacy of the thermophoretic actuation towards the filling of narrow capillaries under the influence of a thermal gradient.

Keywords: Microchannel, Nanofluid, Suspension, Thermophoresis, Capillary transport

## 1. Introduction

Capillary-driven systems are ubiquitous in this physical world, with implications in diverse applications ranging from the transport of blood in the cardio-vascular pathways to the ascent of sap in plants occurring through the xylem and phloem tissues. Capillary transport has also been a widely pursued problem in the field of microfluidics (Dhar et al., 2016; Chakraborty et al., 2009; Dutta and Beskok, 2001; Bandopadhyay et al., 2014; Sarkar and Ganguly, 2015; Jain and Chakraborty, 2010; Bandopadhyay et al., 2017). Microfluidic transport has widespread importance, encompassing biomedical engineering to flow-modulated cooling of electronic components and also in chemical process engineering (Hu et al., 2017; Elvira et al., 2013; Drummond et al., 2016; Kar et al., 2016; Weibel and Garimella, 2012; Magro et al., 2017; Dey et al., 2015; Clark and Abate, 2017). Pressure driven microfluidic transport has several disadvantages which include paucity of precise experimental control, high pumping power requisites and ample dispersion. This has led to the emergence of various other modes of transport which include electroosmosis, magnetohydrodynamics, and electrokinetics. Various state of the art models (Das and Chakraborty, 2006; Waghmare and Mitra, 2012; Chakraborty, 2007; Gunda et al., 2013; Dhar et al., 2015; Rawool et al., 2006; Desai et al., 2014; Sharma and Chakraborty, 2008; Saha et al., 2009; Bandopadhyay and Chakraborty, 2012) are available in this regard with an attempt to understand the physics of flow of Newtonian as well as Non-Newtonian fluids in presence of different forcing conditions.

Because of the immense diversity of the environments where capillary flows prevail, they are subjected to different physical forcing conditions arising from their surroundings. In this context, the detailed analysis of the physics of capillary flows attains paramount importance as it not only provides extremely useful theoretical insights to intricacies of the physical phenomenon by eliciting valuable scientific implications, but also leads to the development of devices with widespread practical applications.

When there is a temperature gradient in a particle-laden fluid subjected to capillarity, the particles suspended in the fluid experience a force on account of thermophoresis (Talbot et al., 1980). Such thermophoretic force has been a driving factor behind the deposition of particles in a gaseous medium leading to commonly observed phenomena like blackening of a lantern. Based on particle sizes, different particles will experience different forces in presence of thermal gradients in a given flow field. Such thermal gradients, however, are

prevalent in most of the modern day lab-on-a-chip devices and they may be pertinently utilized to regulate the resultant capillary dynamics, resulting in varied migration rates of the particles (Malvandi and Ganji, 2014; Guha and Samanta, 2014). In principle, temperature gradients existing in a system can be employed to separate different particles in a suspension.

Choi and Eastman (1995) coined the neologism “nanofluid” as a dilute mixture of particles, varying in size from 1 nm to 100 nm, suspended in a base fluid. Compared to base fluids, nanofluids inimitably possess superior thermophysical attributes like thermal conductivity (Choi and Eastman, 1995). Previously, thermophoretic effects in nanofluids have been studied with a motivation to explore interesting phenomena involving such suspensions including critical heat fluxes in boiling condition, magneto hydrodynamic effects on convection, heat transfer enhancement in convective flows, hydrodynamics in presence of varied driving forces and confinements (Khan et al., 2017; Ganguly et al., 2015; Sheikholeslami et al., 2015; Bahiraei et al., 2013; Ullah et al., 2017; Pradhan et al., 2014; Malvandi et al., 2016; Sarkar et al., 2016). In microscale engineering systems like heat pipes and cooling components of electronic devices, where appreciable thermal gradients prevail, nanofluids can be utilized for their enhanced thermophysical properties. Consequently, the study of thermophoretic effects on the transport of nanofluids in these confinements is of utmost importance, and has not been addressed in detail.

This paper deals with the effects of thermophoresis on the capillary filling dynamics of nanofluids. The primary focus is to mathematically investigate the dynamics of capillary flow of nanofluids in the presence of thermal gradients, using a reduced order model, addressing the following: a) effect of particle size, b) influence of thermal gradient. Furthermore, the work is motivated by the requirement to achieve nanoparticle separations accompanied by a critical exegesis of the influence of pertinent parameters on nanoparticle deposition in in microfluidic confinements.

In the following section, the mathematical model used to illustrate the above-mentioned physical aspects is discussed in detail, along with the relevant fundamental parameters that implicitly influence the interaction of the various important facets controlling the physics of flow.

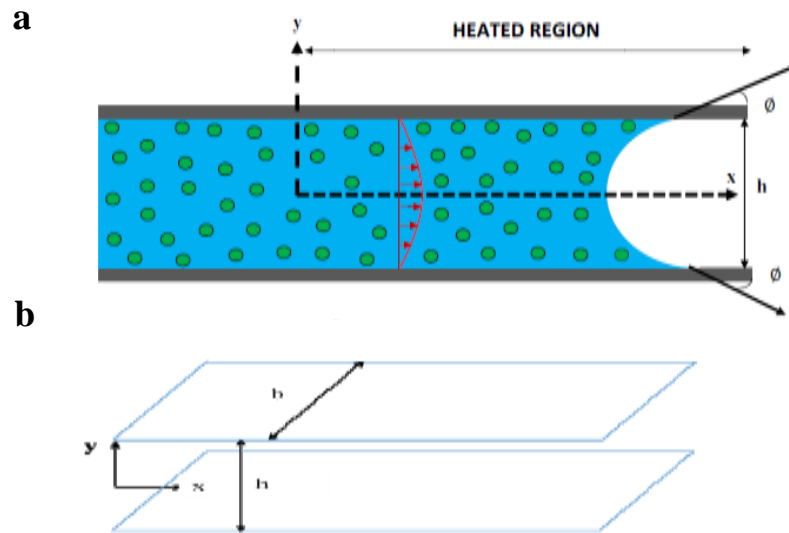


**Fig. 1.**(a) Schematic depicting the layout of the computational domain, **(b)** Symbolic dimensions assuming an idealized parallel plate channel geometry

## 2. Mathematical formulation

### 2.1. Physical problem

We consider parallel plate microchannel geometry, with the two plates being separated by a distance  $h$  which is equal to  $500 \mu\text{m}$ . The channel is assumed to have a width  $b$  perpendicular to the plane of the diagram, such that  $b \gg h$  (refer to Fig. 1b). The fluid initially crosses the perfectly insulated section (refer to Fig. 1a, where a small part of the insulated region is shown) and the insulated section is long enough for the flow to become hydrodynamically fully developed. We set our origin at the center of the channel in the beginning of the heated section (see Fig. 1(a)), with  $y$  axis running along the transverse direction and  $x$  axis along the length of the channel. The static contact angle at the solid-liquid-gas (air) interface is denoted by  $\phi$ . There will be a transition of the fully developed velocity profile to a meniscus traction regime near the interface via a transition region. However, the length of

this meniscus traction regime is very small compared to the length of the fully developed region and hence, is neglected in this model.

At the inlet of the heated section, we have uniform temperature profile and fully developed velocity profile. The nanofluid under consideration conceived as a suspension of nanoparticles comprises two discrete phases-1) The liquid phase (water) 2) The particle phase ( $\text{SiO}_2$ ). One of the most important considerations of the present model is that there is uni-directional coupling (i.e. the particle motion is determined by the flow field not the other way around) and there will be no mutual interaction between the particles (Guha and Samanta, 2014). The potency of this assumption is attributed to the fact that we will be dealing with nanofluids of extremely dilute concentrations ( $C \sim 10^{-3} \text{M}$ ) and nanoparticles of sizes ( $d \sim 1 \text{nm}$ ), resulting in low volume fraction ( $\phi \sim 0.001\%$ ). In the current study, gravity, inter-particle forces, magnetic and electrostatic forces on the particle are all neglected. The temperature dependence of viscosity is suitably taken into account in the present model through its dependence on the mean temperature at a given cross-section. Consequently, it is a function of the axial coordinate ( $x$ ) only. Except viscosity, other thermo-physical properties of the fluids are evaluated at the average of the maximum and minimum temperatures. The temperature dependence of thermophysical properties of the fluid is given by Eq. (A.1-4). The thermophysical property of a given nanofluid like thermal conductivity, heat capacity, dynamic viscosity was computed as a function of the particle volume fraction ( $\phi$ ) by He et al. (2009). Later, Ganguly et al. (2015) incorporated established models to obtain pertinent thermophysical properties of the nanofluids in their study. However, in the limit of low volume fractions, the thermophysical property of a nanofluid becomes equivalent to the corresponding property of the fluid phase. Hence, in the present analysis, the nanofluid properties have been replaced by the analogous properties of the fluid phase.

## 2.2. Model for capillary transport

Here, we apply a reduced order model (Chakraborty, 2005) that is commonly used for evaluating the capillary filling distance as a function of time. This model has its inception from the early works of Lucas (1918) and Washburn (1921). By dynamics of the capillary transport following this model, what we intend to study is the average position ( $x$ ) of the capillary front at a time  $t$ . The equation of motion for the capillary advancement taking the

appropriate direction of the forces, following Newton's second law of motion, may be expressed as (neglecting inertial forces consistent with a microfluidic paradigm):

$$F_{ST} + F_V(x) + F_T(x) = 0 \quad (1)$$

Where  $F_{ST}$ ,  $F_V(x)$  and  $F_T(x)$  denote forces due to surface tension, viscous resistance at the walls and thermophoresis respectively.

### 2.3. Model for forces acting on the nanofluid

The force due to surface tension is modelled by assuming static contact angle and neglecting the dependence of surface tension coefficient on interfacial particle concentration. The walls of the microchannel being kept at uniform temperature, surface tension coefficient is independent of temperature. We have also tested for results with dynamic contact angle and no qualitative changes in the results have been observed. That is why, for simplicity yet without sacrificing the essential physics that we intend to capture, we account for static contact angle only.  $F_{ST}$ , thus, can be expressed as:

$$F_{ST} = \sigma P \cos \phi \quad (2)$$

where  $\sigma$  stands for the surface tension coefficient of the liquid,  $P$  denotes the perimeter of the cross-section of the microchannel and  $\phi$  stands for the static contact angle of the liquid-channel interface and is chosen as  $40^\circ$  in the present study.

The modelling of the viscous force necessitates the requirement of knowledge of the velocity gradients in the flow. For this purpose, the following expression of the axial velocity variations, considering hydrodynamically fully developed flow in a local sense, is used:

$$\frac{u(x, y)}{u_{avg}(x)} = \frac{3}{2}(1 - 4y^2) \quad (3)$$

$$\frac{u_{avg}(0)}{u_{avg}(x)} = \frac{\mu_l(x)}{\mu_l(0)} \quad (4)$$

$$F_V(x) = \frac{12\mu_l(x)\dot{x}xb}{h} \quad (5)$$

Here,  $u_{avg}(x)$  refers to the average inlet velocity at any particular cross-section,  $\dot{x}$  stands for the velocity of the capillary front, where  $x$  is the instantaneous position of capillary front from the origin of the reference coordinate system, and  $\mu_l(x)$  is the dynamic viscosity of the fluid.

The thermophoretic force acts on the particles as a consequence of the temperature gradient existing in the flow. Thermal gradients in the flow result in the concentration gradients. Thermal gradients coupled with the concentration gradients give rise to the thermophoretic force. The thermophoretic force acting against the temperature gradient at a given point on a given particle is directly proportional to the temperature gradient at that point and is inversely proportional to the local temperature (He et al., 2009). The constant of proportionality, known as the thermophoretic coefficient, depends on the axial coordinate because of its dependence on the dynamic viscosity. Estimation of the thermophoretic force necessitates the knowledge of temperature distribution  $T(x,y)$  and resulting particle distribution in the fluid  $C(x,y)$ . We can express the total thermophoretic force with the help of the following expression:

$$F_T(x) = - \int_0^x \int_{-\frac{h}{2}}^{\frac{h}{2}} D_{T,p}(x) \frac{\partial T}{\partial x} \frac{C(x,y)}{T(x,y)} b dx dy \quad (6)$$

$$D_{T,p}(x) = \frac{6\pi d_p \mu_l(x)^2 C_s (K + C_t Kn)}{\rho_l (1 + 3C_m Kn)(1 + 2K + 2C_t Kn)} \quad (7)$$

Here,  $D_{T,p}(x)$  stands for the thermophoretic coefficient. Definition of the same may be found in the study of thermophoresis of particles in heated boundary layer by Talbot et al. (1980). The negative sign implies that the force acts against the temperature gradient.  $C_m$ ,  $C_s$ ,  $C_t$  are the momentum exchange coefficient, thermal slip coefficient and the temperature jump coefficient, and are taken to be equal to 1.146, 1.147 and 2.18, respectively (He et al., 2009).  $K$  is the ratio of the working fluid thermal conductivity  $k_l$ , computed from Eq. (A.3), and the particle thermal conductivity  $k_p$ , in the present working temperature range of 278 K to 323 K, is treated as a constant which equals 1.38 W/mK.  $Kn$  denotes the Knudsen number and is defined as  $Kn = 2\lambda/d$ , where  $\lambda$  stands for the mean free path of the working fluid and  $d$  denotes the diameter of the nano-particles. Particles ranging from sizes 1 nm to 5 nm are considered in the present study.



#### 2.4. Governing equations of temperature and particle concentration fields

For the calculation of temperature field, quasi steady-state approximation and negligible axial conduction in conjunction with no viscous dissipation and work-transfer is considered. The effect of variation of dynamic viscosity with temperature is also accounted for. The walls of the microchannel are heated to identical constant temperature ( $T_w$ ). The energy equation now can be written in terms of the non-dimensional temperature  $\theta(x, y)$  as:

$$\theta(x, y) = \frac{T(x, y) - T_w}{T_w} \quad (8)$$

$$\frac{u(x, y)}{u_{avg}(0)} \frac{\partial \theta}{\partial x} = \frac{1}{Pe} \frac{\partial^2 \theta}{\partial y^2} \quad (9)$$

$Pe$  stands for the Peclet number of the flow and is given by  $Pe = RePr$ , where  $Re$  denotes the Reynolds number of the flow at the inlet and  $Pr$  is the Prandtl number of the fluid being calculated at the average of the maximum and minimum temperatures. Here,  $u_{avg}(x)$  stands for the average velocity of flow. Eq. (9) can be solved numerically with boundary conditions:

$$\theta|_{\bar{y}=-1/2} = 0 \quad \forall \quad 0 < \bar{x} < \bar{l} \quad (10a)$$

$$\theta|_{\bar{y}=+1/2} = 0 \quad \forall \quad 0 < \bar{x} < \bar{l} \quad (10b)$$

$$\theta|_{\bar{x}=0} = \theta_i \quad \forall \quad -\frac{1}{2} < \bar{y} < \frac{1}{2} \quad (10c)$$

$\bar{x}$ ,  $\bar{y}$  and  $\bar{l}$  are the non-dimensionalised versions of  $x$ ,  $y$  and  $l$  after being normalized by  $h$ .  $\theta_i$  stands for the non-dimensional version of the inlet temperature. The inlet temperature is kept fixed at 323K for the water-SiO<sub>2</sub> nanofluid considered in the entire study, and the wall temperature is varied from 278 K to 323 K, thereby varying the inlet non-dimensional temperature.

For the computation of concentration field, we adopt quasi steady-state approximation along with minimal axial diffusion. Particle velocity in the convective term is replaced by the axial velocity of the fluid, as the particle size is in the order of nm. There is an additional term appearing in the species conservation equation due to the thermophoretic effect (Guha and Samanta, 2014; Chein and Liao, 2005). Concentration of particles near the wall in the

fluid is taken as zero, as we have assumed that particles adhere to the wall as they impinge on the wall. This assumption is ideally applicable for particles having sizes less than 2 nm, but has been used for particles of sizes as large as 10 nm (Chein and Liao, 2005). In the present study, we are confining ourselves to the maximum particle size of 5 nm. Hence, the species conservation equation can be written in terms of non-dimensional concentration  $\bar{C}(x, y)$  as:

$$\bar{C}(x, y) = \frac{C(x, y)}{C_0} \quad (11)$$

$$\frac{u(x, y)}{u_{avg}(0)} \frac{\partial \bar{C}}{\partial x} = \frac{1}{Pe_c} \frac{\partial^2 \bar{C}}{\partial y^2} + \frac{K_{T,P}}{Re} \frac{\partial}{\partial y} \left( \frac{\bar{C}}{1+\theta} \frac{\partial \theta}{\partial y} \right) \quad (12)$$

Here  $C_0$  is the concentration of particles at the inlet of the channel.  $C_0$  is taken to be 1 mM/m<sup>3</sup> for the study.  $Pe_c$  stands for the particle Peclet number and is given by  $Pe_c = ReSc$ , where  $Re$  denotes the Reynolds number of the flow at the inlet and  $Sc$  is the Schmidt number of the fluid being calculated at the average of the maximum and minimum temperatures.  $K_{T,P}$  in this equation stands for the thermophoretic coefficient for the concentration term which is denoted by:

$$K_{T,P} = \frac{2C_s C_c (K + C_t Kn)}{(1 + 3C_m Kn)(1 + 2K + 2C_t Kn)} \quad (13)$$

Where  $C_c$  is the equivalent Cunningham correction factor in the present case, similar to the expression given by Chein and Liao (2005).

$$C_c = 1 + Kn \left[ 1.257 + 0.4 \exp\left(\frac{-1.1}{Kn}\right) \right] \quad (14)$$

The particle diffusivity  $D$ , evoking Stokes Einstein theory, is estimated as:

$$D = \frac{C_c}{3\pi d \mu_{avg}} k_B T_{avg} \quad (15)$$

The Schmidt number takes the form:

$$Sc = \frac{\mu_{avg}}{\rho_l D} \quad (16)$$

In Eq. (15),  $k_B$  stands for the Boltzmann constant and is equal to  $1.38 \times 10^{-23}$ .  $\mu_{avg}$  and  $\rho_l$  are the dynamic viscosity and density at  $T_{avg}$  which is the average of the maximum and minimum temperatures. The relevant boundary conditions are as follows:

$$\bar{C}|_{\bar{y}=-1/2} = 0 \quad \forall \quad 0 < \bar{x} < \bar{l} \quad (17a)$$

$$\bar{C}|_{\bar{y}=+1/2} = 0 \quad \forall \quad 0 < \bar{x} < \bar{l} \quad (17b)$$

$$\bar{C}|_{\bar{x}=0} = 1 \quad \forall \quad -\frac{1}{2} < \bar{y} < \frac{1}{2} \quad (17c)$$

Eq. (9) is solved numerically along with relevant boundary conditions as given by Eq. (10a-c). The inlet conditions being known, first the temperature profile is computed in the consecutive grid points in the axial direction. The mean temperature ( $\bar{T}$ ) at any given axial location is subsequently computed by the following relation:

$$\bar{T}(\bar{x}) = \int_{-\frac{1}{2}}^{+\frac{1}{2}} T(\bar{x}, \bar{y}) d\bar{y} \quad (18)$$

The viscosity is then calculated from Eq. (A.1). This forward marching scheme is repeated for the subsequent grid points. Hence, the solution of the energy equation yields the temperature variation as well as the axial variation of viscosity. Now, Eq. (11) is solved numerically with pertinent boundary conditions as given by Eq. (17a-c), evoking the computed temperature gradients and the viscosity variation, from Eq. (9). The computed temperature and concentration fields are subsequently utilised to calculate the thermophoretic force using Simpson's (1/3<sup>rd</sup>) rule of numerical integration.

Having computed all the forces, Eq. (1) can be rewritten as:

$$\sigma P \cos \phi + F_T(x) - \frac{12\mu_l(x)\dot{x}xb}{h} = 0 \quad (19)$$

As mentioned earlier, the width of the microchannel perpendicular to the plane of the flow ( $b$ ) is taken to be sufficiently large compared to the height ( $h$ ) of the microchannel. The width ( $b$ ) appears only in the surface tension term where we get a ratio of the perimeter ( $P$ ) and the area

(A) which can be tackled by taking the mathematical limit as  $b \rightarrow \infty$ . Hence, Eq. (19) takes the form:

$$\int_0^x \frac{dx}{p(x)} = t \quad (20)$$

where,

$$p(x) = \frac{\sigma h \cos \phi}{6x\mu_l(x)} + \frac{C_0 F(x) h^2}{12x\mu_l(x)} \quad (21)$$

Eq. (20) is solved numerically using Simpson's (1/3<sup>rd</sup>) rule of numerical integration. Here  $F(x)$  is the normalised thermophoretic force and is expressed as:

$$F(x) = \frac{F_T(x)}{C_0 b h} \quad (22)$$

Where  $F_T(x)$  is given by Eq. (6).

### 3. Results and discussion

#### 3.1. Mesh independence and validation of current solution scheme

Outputs should not depend on mesh dimensions; hence, several grids were tested. The transverse concentration profiles at  $\bar{x} = 1.25$  corresponding to  $d = 3$  nm and  $T_w = 278$  K are depicted in Fig. 2. The average non-dimensional concentration ( $\bar{C}_{avg}$ ), corresponding to a particular grid size is calculated and the results are shown in Table 1. Based on the tabulated results, a grid size of  $40 \times 35\ 000$  is selected for the water-SiO<sub>2</sub> nanofluid. The nature of equations for evaluating the temperature and concentration profiles being similar to those used by Chein and Liao (2005), the validation of the numerical technique has been checked by treating viscosity as a constant in the current model and by using the same parameters as used by Chein and Liao (2005) for air-SiO<sub>2</sub> nano-particle suspension. Fig. 3 depicts the accuracy of the current solution scheme relative to the existing numerical results.

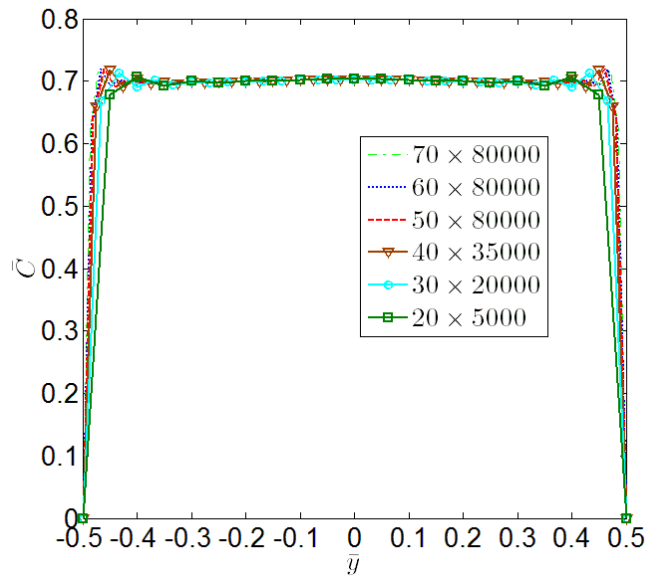


**Fig. 2.** Grid dependency test results at  $\bar{x}=1.25$  with  $d = 3$  nm at  $T_w = 278$  K.

**Table 1**

Comparison of the average non-dimensional concentration  $\bar{C}_{avg}$  for different grid resolution at  $\bar{x}=1.25$  with  $d = 3$  nm at  $T_w = 278$  K

$$\bar{C}_{avg} = \int_{-\frac{1}{2}}^{+\frac{1}{2}} \bar{C}(\bar{x}=1.25, \bar{y}) d\bar{y}$$

Mesh size	20 × 5000	30 × 20 000	40 × 35 000	50 × 80 000	60 × 80 000	70 × 80 000
$\bar{C}_{avg}$	0.6735	0.6811	0.6850	0.6873	0.6888	0.6898

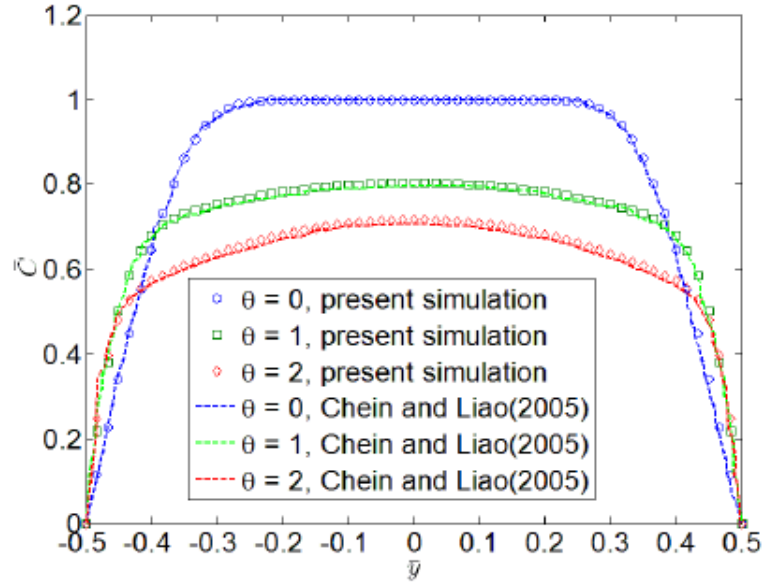


**Fig. 3.** A comparison of the predicted transverse concentration profile with the numerical results reported by Chein and Liao (2005).

### 3.2. Thermal characteristics

As the wall temperature approaches the temperature of the incoming fluid, there is a decrement in the length of the thermal developing region which affects the axial variation of the dynamic viscosity. Consequently, the mean temperature of the fluid decreases and the flow approximately attains the wall temperature. Viscosity of the fluid being inversely dependent on the temperature increases in the thermally developing region and becomes constant and viscosity variations gradually lose prominence as the wall temperature approaches the temperature of the incoming fluid. In the present scenario, thermal gradients are appreciable up to  $\bar{x} = 2$  for the maximum temperature gradient case. Fig. 4 and Fig. 5 depict the axial variation of the mean temperature and viscosity of the fluid, respectively. Hence, the temperature and subsequently the particle concentration profiles are calculated up to  $\bar{x} = 5$ , as beyond that thermophoretic effects become negligible.

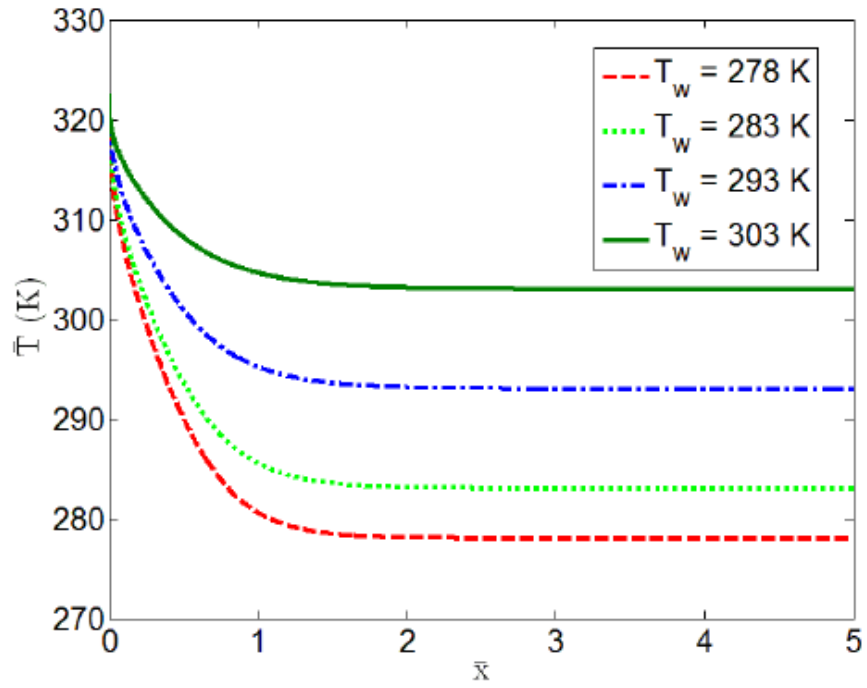


**Fig. 4.** Axial variation of the mean temperature of the fluid, for different wall temperatures

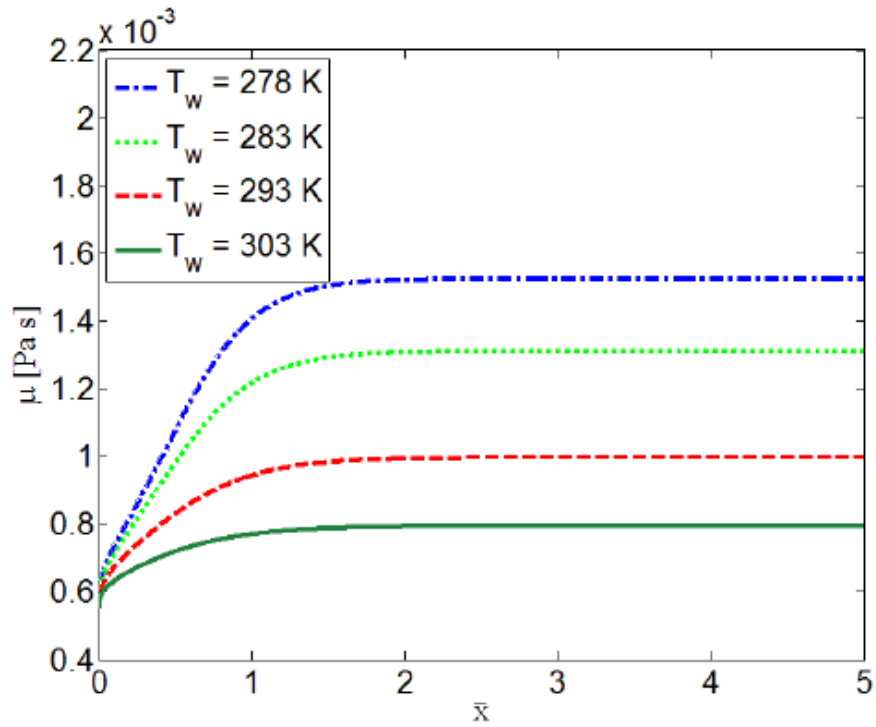


**Fig. 5.** Axial variation of the viscosity of the fluid, for different wall temperatures

### 3.3. Particle concentration fields

Due to the inherent symmetry of the problem in terms of the boundary conditions, the particle concentration profiles are symmetric about the central axis of the microchannel; see Fig. 6. The concentration gradient near the wall decreases as we traverse along the axis of the microchannel due to the gradual development of the particle concentration profile. Increased contact length of the fluid with the wall effects in enhanced thermophoretic particle deposition on the channel walls, inhibiting particle concentrations at a given transverse location as we traverse axially. Concentration profiles for a given nanofluid in a specified confinement, subjected to a particular temperature field, clearly depict that with gradual increase in length along the central axis, accretion in thermophoretic effects diminish. This phenomenon is ascribed to the eventual depletion of thermal gradients, as the capillary front progresses.

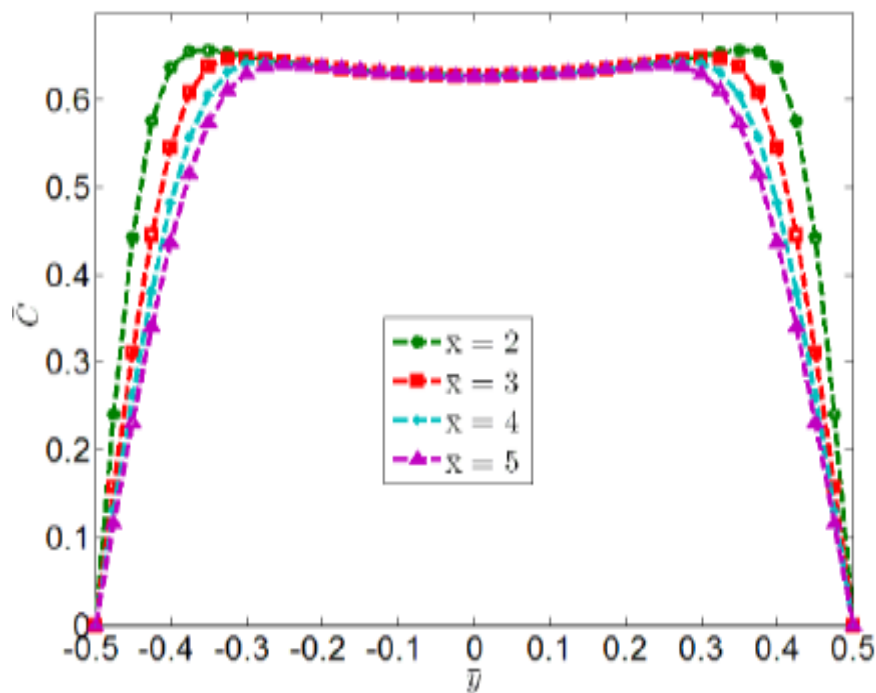


**Fig. 6.** Concentration profiles at various axial and transverse locations, at  $T_w = 278$  K, with  $d = 3$  nm.

Fig. 7 depicts the variations in the concentration profiles for different wall temperatures, corresponding to  $\bar{x} = 5$ , for  $d = 3$  nm. Thermophoretic effects become subdued



with the increase in the wall temperature due to the reduction of axial temperature gradients in the system and particle diffusion becomes the dominant phenomenon. Consequently, thermophoretic particle deposition reduces, leading to higher accumulation of particles near the central axis of the microchannel. The reliance of the particle retaining capacity of the nanofluid on the interplay between thermophoresis and molecular diffusion implies that, in a given microfluidic confinement, particle deposition can be pertinently tailored by modulating the externally imposed thermal gradients. Consequently, this attains utmost importance in nanofluid based microscale engineering applications where particle deposition exceeding a given threshold will be detrimental to the performance of the system.

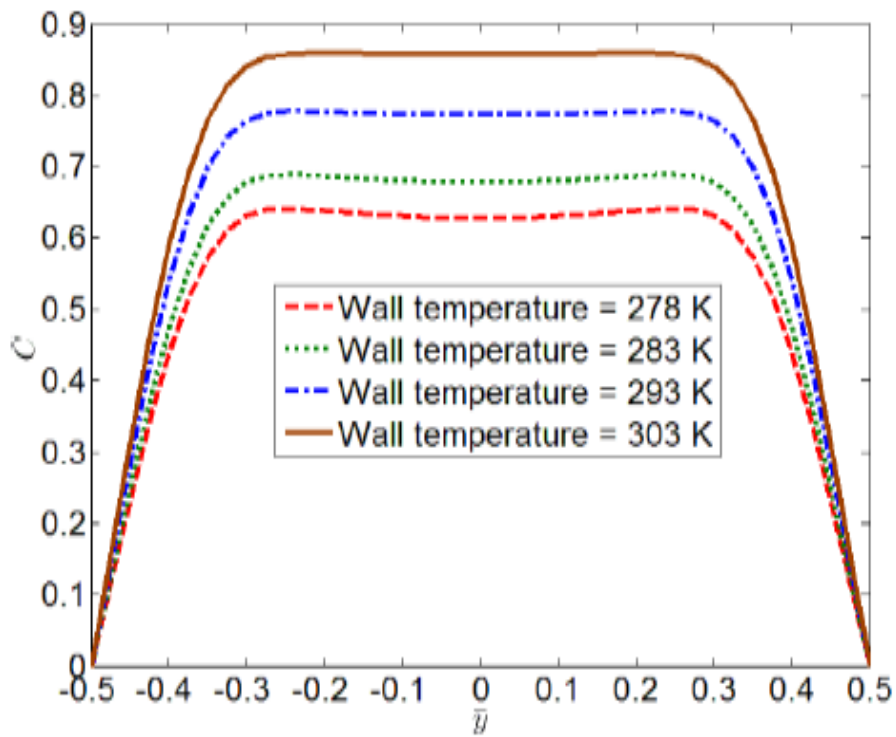


**Fig. 7.** Transverse concentration profiles at  $\bar{x} = 5$  for  $d = 3$  nm, at different wall temperatures.

For a specified wall temperature ( $T_w = 278$  K), concentration profiles at  $\bar{x} = 5$  are depicted for different particle sizes ranging from 1 nm to 5 nm, in Fig. 8. The particle size is reflected in the Schmidt number in the species conservation equation. Increase in Schmidt number ( $Sc$ ) undermines the diffusion phenomena compared to thermophoresis and thereby leads to the increase in concentration gradients near the wall for larger particles; see Fig. 8. In the limiting case when thermophoresis is negligible for lower particle sizes, diffusion is the

predominant phenomenon. It can be inferred that smaller nanoparticle deposition is driven by diffusion contrary to larger nanoparticle deposition, which is dictated by thermophoresis. The transition from diffusion dominated particle deposition to the thermophoretically dominated regime, in turn, determines the particle bearing capacity of the suspension. Consequently, the particle retaining efficacy of a given nanofluid can be suitably exploited to design ancillary particle retrieval systems in diverse engineering applications deploying nanofluids in microscale confinements.

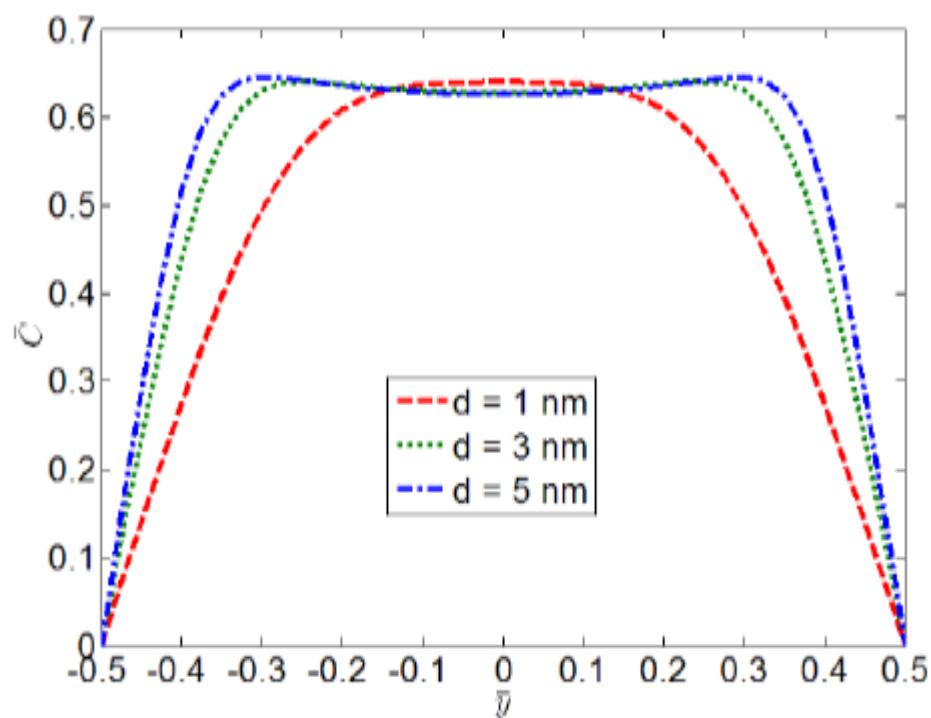


**Fig. 8.** Transverse concentration profiles at  $\bar{x} = 5$  for different particle diameters, at  $T_w = 278$  K

### 3.4. Influence of particle size and wall temperature on thermophoresis and capillary dynamics

The variation of normalised thermophoretic force as a function of the axial coordinate is analysed for particles of different sizes at a fixed wall temperature (278 K); see Fig. 9. The thermophoretic force exhibits an increasing trend up to  $\bar{x} = 2$  and then attains a constant value. This can be explained from the fact that the flow becomes approximately thermally

fully developed after  $\bar{x} = 2$ . Thermophoretic force increases with increase in particle size for a given thermal gradient; this is in concurrence with the results depicted before in this paper.

Fig. 10 depicts the capillary filling characteristics, as a function of the particle size. With increase in particle size, the thermophoretic force increases and consequently, the nanoparticle suspension takes lesser time to traverse a given length of the channel ( $\bar{x} = 5$ ). It can be noted that the increase in capillary filling is comparatively higher for lower particle size. This is primarily attributed to the higher relative increase in the thermophoretic force at lower particle size. The influence of particle size on capillary dynamics can be utilized to achieve separation of nanoparticles in a heterogeneous nanofluid.

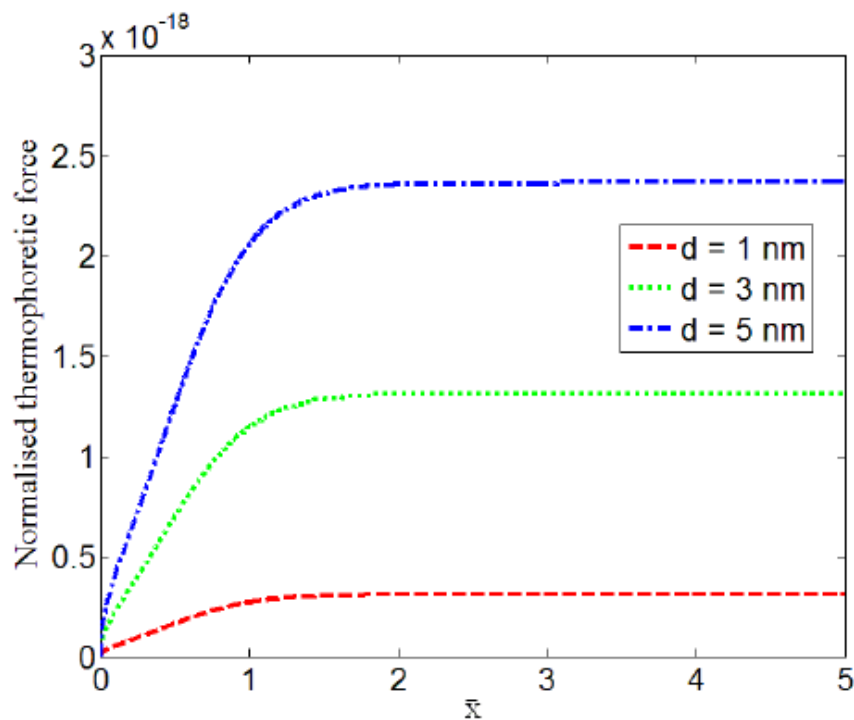


**Fig. 9.** Variation of normalised thermophoretic force with axial position for different particles at  $T_w = 278$  K

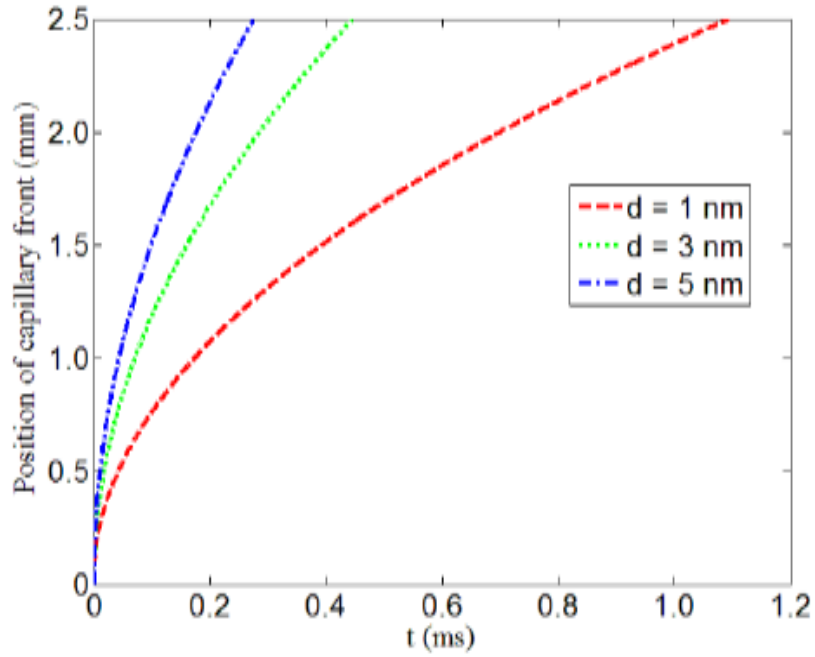


**Fig. 10.** Comparison between thermophoretically driven capillary transport for different particle sizes at  $T_w = 278$  K

The variation of normalised thermophoretic force as a function of the axial coordinate is analysed for different wall temperatures for a fixed particle size of 3 nm; see Fig. 11. The magnitude of the thermophoretic force decreases with the increase in the wall temperature which is attributed to the decrease in the temperature gradients in the flow. Moreover, with increase in the wall temperature, the fluid attains thermal equilibrium with the wall over a shorter length. Consequently, there is reduction of the length over which there is appreciable variation of thermophoretic force.

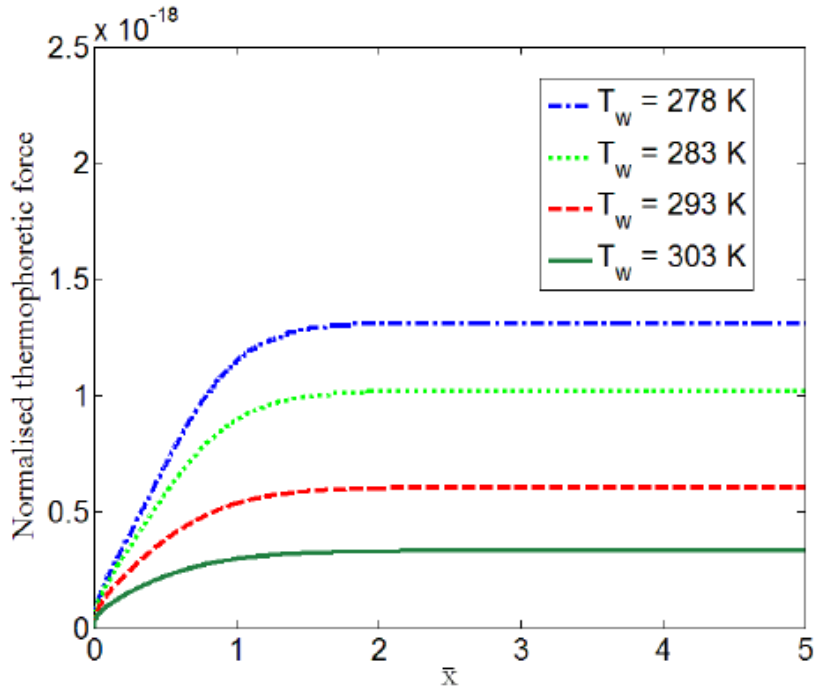


**Fig. 11.** Variation of normalised thermophoretic force with axial position for  $d = 3$  nm at different wall temperatures

As the wall temperature approaches the temperature of the incoming fluid, at a given time the axial displacement of the nanofluid decreases. This is in consensus with the gradual reduction of thermophoretic force with increase in wall temperature for a specific temperature of the incoming fluid (323 K) and fixed particle dimension in the suspension. Thermophoresis clearly enhances the axial rate of transport as compared to purely surface tension driven transport; see Fig. 12. It is worthwhile to note here, that beyond a particular wall temperature for identical inlet conditions, the rate of capillary transport does not increase significantly. Hence, optimum flow rates do exist for a particular incoming nanofluid in a given microfluidic confinement.

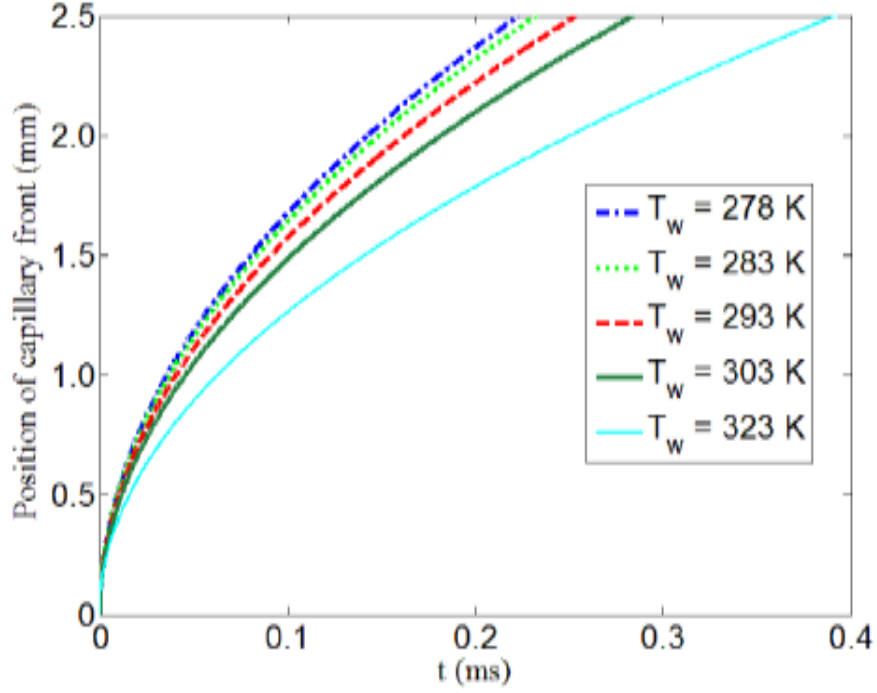


**Fig. 12.** Comparison between thermophoretically driven capillary transport at different wall temperatures and purely surface tension driven transport, corresponding to  $d = 3$  nm.

#### 4. Conclusions

A general transport model of the nanofluid has been developed in presence of thermophoretic force for explicating particle migration in fluid medium and eventually delineating the evolving capillary dynamics. A uni-directional coupling between the energy equation and species conservation equation has been aptly considered, with the incorporation of the effect of thermophoresis in the species conservation equation. The most important feature of the present mathematical model is the judicious inclusion of the temperature dependence of viscosity. Findings reveal the existence of two discrete phenomena governing particle transport, dictated by the particle size for a prescribed thermal gradient, namely-diffusion and thermophoresis; the interplay between them influences particle deposition, thereby modulating the particle retaining potential of the nanofluid. In conclusion, thermal gradients in a confinement exacerbate the particle bearing capability of a particular nanofluid. Moreover, the current model elucidates the effects of thermal gradients and particle sizes on the transport of the nanofluid. One of the most important outcomes of this mathematical model is that in practice, nanoparticle separation can be achieved by employing thermal gradients in a heterogeneous suspension. It is explicitly demonstrated that thermophoresis clearly enhances the rate of transport relative to purely surface-tension driven capillary

transport. Furthermore, for a given particle size, thermophoretic force, and consequently, the resultant capillary dynamics gets influenced by the presence of thermal gradients in the system. In this respect, by the appropriate control of channel wall temperature, one can attain optimum rates of transport, reducing the energy costs.

## Appendix A

The thermophysical properties of water obtained from the ASHRAE Handbook were utilized to fit a curve for computing the properties at any given temperature  $T$  in our working range (278 K – 323 K).

*-Thermophysical properties of water*

$$\mu_l = -0.0000000064998705T^3 + 0.0000062619509380T^2 - 0.0020209918320204T + 0.2190624024917910 \quad (1)$$

$$\rho_l = 0.000031456953644T^3 - 0.033012426316595T^2 + 11.038660196122500T - 193.285493540877000 \quad (2)$$

$$k_l = 0.00000022710464T^4 - 0.00027624146191T^3 + 0.12595124064798T^2 - 25.51100962753100T + 1,937.27799984267000 \quad (3)$$

$$Pr = -0.00007726338280T^3 + 0.07311004221889T^2 - 23.14366046554400T + 2,455.08343412100000 \quad (4)$$

## Conflict of interest

The authors of this manuscript have no conflict of interest.

## References

- Bahiraei, M., Hosseinalipour, S.M., Morteza, H., (2013). Laminar forced convection of a water-TiO<sub>2</sub> nanofluid in annuli considering mass conservation for particles. Chem. Eng. Technol. 36, 2057-2064. <https://doi.org/10.1002/ceat.201300382>
- Bandopadhyay, A., Chakraborty, S., (2012). Electrokinetically induced alterations in dynamic response of viscoelastic fluids in narrow confinements. Phys. Rev. E. 85, 056302. <https://doi.org/10.1103/PhysRevE.85.056302>
- Bandopadhyay, A., Ghosh, U., Chakraborty, S., (2014). Capillary filling dynamics of viscoelastic fluids. Phys. Rev. E. 89, 053024. <https://doi.org/10.1103/PhysRevE.89.053024>

Bandopadhyay, A., Mandal, S., Chakraborty, S., (2017). Capillary transport of two immiscible fluids in presence of electroviscous retardation. *Electrophoresis*. 38, 747-754. <https://doi.org/10.1002/elps.201600395>

Chakraborty, D., Gorkin, R., Madou, M., Kulinsky, L., Chakraborty, S., (2009). Capillary filling in centrifugally actuated microfluidic devices with dynamically evolving contact line motion. *J. Appl. Phys.* 105, 084904. <http://dx.doi.org/10.1063/1.3110016>

Chakraborty, S., (2007). Electroosmotically driven capillary transport of typical non-Newtonian biofluids in rectangular microchannels. *Anal. Chim. Acta*. 605, 175-184. <https://doi.org/10.1016/j.aca.2007.10.049>

Chakraborty, S., (2005). Dynamics of capillary flow of blood into a microfluidic channel. *Lab Chip*. 5, 421-430. <https://dx.doi.org/10.1039/B414566F>

Chein, R., Liao, W., (2005). Thermophoretic effects on nano-particle deposition in channel flow. *Heat Mass Transf.* 42, 71-79. <https://doi.org/10.1007/s00231-005-0662-5>

Choi, S.U.S., Eastman, J.A., 1995. Enhancing thermal conductivity of fluids with nanoparticles. *Proc. 1995 ASME Int. Mech. Engineering Congr. Expo.*

SanFrancisco, USA, ASME, FED231/MD66 99–105.

Clark, I., Abate, A.R., (2017). Finding a helix in a haystack: nucleic acid cytometry with droplet microfluidics. *Lab Chip*. (2017). <https://doi.org/10.1039/C7LC00241F>

Das, S., Chakraborty, S., (2006). Analytical solutions for velocity, temperature and concentration distribution in electroosmotic microchannel flows of a non-Newtonian biofluid. *Anal. Chim. Acta*. 559, 15-24. <https://doi.org/10.1016/j.aca.2005.11.046>

Desai, N., Ghosh, U., Chakraborty, S., (2014). Capillary filling under electro-osmotic effects in the presence of electromagneto-hydrodynamic effects. *Phys. Rev. E*. 89, 063017. <https://doi.org/10.1103/PhysRevE.89.063017>

Dey, R., Kar, S., Joshi, S., Maiti, T.K., Chakraborty, S., (2015). Ultra-low-cost ‘paper-and-pencil’ device for electrically controlled micromixing of analytes. *Microfluid Nanofluid.* 19, 375-383. <https://doi.org/10.1007/s10404-015-1567-3>

Dhar, J., Ghosh, U., Chakraborty, S., (2015). Electro-capillary effects in capillary filling dynamics of electrorheological fluids. *Soft Matter*. 11, 6957-6967. <https://doi.org/10.1039/C5SM01092F>

Dhar, J., Jaggi, P., Chakraborty, S., (2016). Oscillatory regimes of capillary imbibition of viscoelastic fluids through concentric annulus. *RSC Adv.* 6, 60117-60125. <https://doi.org/10.1039/C6RA05002F>

Drummond, K.P., Weibel, J.A., Garimella, S.V., (2016). Evaporative intrachip hotspot cooling with a hierarchical manifold microchannel heat sink array. *Thermal and*



Thermomechanical Phenomena in Electronic Systems (ITherm), 15th IEEE Intersociety Conference on. IEEE. <https://doi.org/10.1109/ITHERM.2016.7517565>

Dutta, P., Beskok, A., (2001). Analytical solution of time periodic electroosmotic flows: analogies to stokes' second problem. *Anal. Chem.* 73, 5097-5102. .  
<https://doi.org/10.1021/ac015546y>

Elvira, K.S., ISolvas, X.C., Wootton, R.C., (2013). The past, present and potential for microfluidic reactor technology in chemical synthesis. *Nature Chem.* 5, 905-915.  
<https://doi.org/10.1038/nchem.1753>

Ganguly, S., Sarkar, S., Hota, T.K., Mishra, M., (2015). Thermally developing combined electroosmotic and pressure-driven flow of nanofluids in a microchannel under the effect of magnetic field. *Chem. Eng. Sci.* 126, 10-21. <https://doi.org/10.1016/j.ces.2014.11.060>

Guha, A., Samanta, S., (2014). Effect of thermophoresis on the motion of aerosol particles in natural convective flow on horizontal plates. *Int. J. Heat Mass Transf.* 68, 42-50.  
<https://doi.org/10.1016/j.ijheatmasstransfer.2013.08.046>

Gunda, N.S.K., Joseph, J., Tamayol, A., Akbari, M., Mitra, S.K., (2013). Measurement of pressure drop and flow resistance in microchannels with integrated micropillars. *Microfluid Nanofluid.* 14, 711-721. <https://doi.org/10.1007/s10404-012-1089-1>

Handbook, A.S.H.R.A.E., (2005). Fundamentals, American Society of Heating, Refrigerating Air-Condition. Engineers Inc., Atlanta.

He, Y., Men, Y., Zhao, Y., Lu, H., Ding, Y., (2009). Numerical investigation into the convective heat transfer of TiO<sub>2</sub> nanofluids flowing through a straight tube under the laminar flow conditions. *Appl. Therm. Eng.* 29, 1965-1972.  
<https://doi.org/10.1016/j.applthermaleng.2008.09.020>

Hu, B., Li, J., Mou, L., Liu, Y., Deng, J., Qian, W., ... & Jiang, X., (2017). An automated and portable microfluidic chemiluminescent immunoassay for quantitative detection of biomarkers. *Lab Chip.* <https://doi.org/10.1039/C7LC00249A>

Jain, A., Chakraborty, S., (2010). Interfacial ph-gradient induced micro-capillary filling with the aid of transverse electrodes arrays in presence of electrical double layer effects. *Anal. Chim. Acta.* 659, 1-2, 1-8. <https://doi.org/10.1016/j.aca.2009.11.029>

Kar, S., Maiti, T.K., Chakraborty, S., (2016). Microfluidics-based low-cost medical diagnostic devices: some recent developments. *INAE Lett.* 1, 59-64.  
<https://doi.org/10.1007/s41403-016-0009-1>

Khan, M., Azam, M., Munir, A., (2017). On unsteady Falkner-Skan flow of MHD Carreau nanofluid past a static/moving wedge with convective surface condition. *J. Mol. Liq.* 230, 48-58. <https://doi.org/10.1016/j.molliq.2016.12.097>

Lucas, R., (1918). The time law of the capillary rise of liquids. *Kolloid-Zeitschrift.* 23, 15-22.  
<https://doi.org/10.1007/BF01461107>

- Magro, L., Escadafal, C., Garneret, P., Jacquelin, B., Kwasiborski, A., Manuguerra, J.C., ... & Tabeling, P., (2017). Paper microfluidics for Nucleic Acids Amplification Testing (NAAT) of infectious diseases. *Lab Chip*. <https://doi.org/10.1039/C7LC00013H>
- Malvandi, A., Ganji, D.D., (2014). Effects of nanoparticle migration on force convection of Alumina/water nanofluid in a cooled parallel plate channel. *Adv. Powder Technol.* 25, 1369-1375. <http://dx.doi.org/10.1016/j.appt.2014.03.017>
- Malvandi, A., Heysiattalab, S., Ganji, D.D., (2016). Thermophoresis and brownian motion effects on heat transfer enhancement at film boiling of nanofluids over a vertical cylinder. *J. Mol. Liq.* 216, 503-509. <https://doi.org/10.1016/j.molliq.2016.01.030>
- Pradhan, K., Samanta, S., Guha, A., (2014). Natural convective boundary layer flow of nanofluids above an isothermal horizontal plate. *J. Heat Transf.* 136, 102501. <https://doi.org/10.1115/1.4027909>
- Rawool, A.S., Mitra, S.K., Kandlikar, S.G., (2006). Numerical simulation of flow through microchannels with designed roughness. *Microfluid Nanofluid.* 2, 215-221. <https://doi.org/10.1007/s10404-005-0064-5>
- Saha, A.A., Mitra, S.K., Tweedie, M., Roy, S., McLaughlin, J., (2009). Experimental and numerical investigation of capillary flow in SU8 and PDMS microchannels with integrated pillars. *Microfluid Nanofluid.* 7, 451. <https://doi.org/10.1007/s10404-008-0395-0>
- Sarkar, S., Ganguly, S., (2015). Fully developed thermal transport in combined pressure and electroosmotically driven flow of nanofluid in a microchannel under the effect of a magnetic field. *Microfluid Nanofluid.* 18, 623-636. <https://doi.org/10.1007/s10404-014-1461-4>
- Sarkar, S., Ganguly, S., Biswas, G., Saha, P., (2016). Effect of cylinder rotation during mixed convective flow of nanofluids past a circular cylinder. *Comput. Fluids.* 127, 47-64. <https://doi.org/10.1016/j.compfluid.2015.12.013>
- Sharma, A., Chakraborty, S., (2008). Semi-analytical solution of the extended Graetz problem for combined electroosmotically and pressure-driven microchannel flows with step-change in wall temperature. *Int. J. Heat Mass Trans.* 51, 4875-4885. <https://doi.org/10.1016/j.ijheatmasstransfer.2008.02.04>
- Sheikholeslami, M., Ganji, D.D., Javed, M.Y., Ellahi, R., (2015). Effect of thermal radiation on magnetohydrodynamics nanofluid flow and heat transfer by means of two phase model. *J. Magn. Mater.* 374, 36-43. <https://doi.org/10.1016/j.jmmm.2014.08.021>
- Talbot, L., Cheng, R.K., Schefer, R.W., Willis, D.R., (1980). Thermophoresis of particles in a heated boundary layer. *J. Fluid Mech.* 101, 737-758. <https://doi.org/10.1017/S0022112080001905>
- Ullah, I., Shafie, S., Makinde, O. D., Khan, I., (2017). Unsteady MHD Falkner-Skan flow of Casson nanofluid with generative/destructive chemical reaction. *Chem. Eng. Sci.* <https://doi.org/10.1016/j.ces.2017.07.011>

Waghmare, P.R., Mitra, S.K., (2012). A comprehensive theoretical model of capillary transport in rectangular microchannels. *Microfluid Nanofluid.* 12, 53-63. <https://doi.org/10.1007/s10404-011-0848-8>

Washburn, E.W., (1921). The dynamics of capillary flow. *Phys. Rev.* 17, 273. <https://doi.org/10.1103/PhysRev.17.273>

Weibel, J.A., Garimella, S.V., (2012). Visualization of vapor formation regimes during capillary-fed boiling in sintered-powder heat pipe wicks. *Int. J. Heat Mass Transf.* 55, 3498-3510. <https://doi.org/10.1016/j.ijheatmasstransfer.2012.03.021>